Nonlinear detector response of Aqua MODIS land imaging bands

Kevin A. Twedt, Sarah Henderson, Xiaoxiong Xiong, Amit Angal and Xu Geng

***Abstract*— The detectors in Aqua MODIS reflective solar bands (RSB) are calibrated assuming a linear relationship between the observed top-of-atmosphere radiance and the instrument output response. Any non-linear behavior in the system response can contribute to errors in NASA's Level 1B MODIS reflectance and radiance products, which are used in a wide variety of Earth science applications. While most RSB detectors continue to have very linear behavior even after more than 18 years of operation, we present evidence that the detectors in Aqua MODIS bands 1 (645 nm) and 2 (858 nm) have deviations from gain linearity that change over the mission by up to 3%. We show a clear divergence between gain measurements made with the on-board solar diffuser (SD) at two different radiance levels, achieved by collecting data both with and without an attenuation screen. Radiance trends from lunar calibrations and typical desert and ocean scenes are also compared. We present a simple method to characterize the response non-linearity using a quadratic function by combining the results of the two sets of SD calibrations. Applying this quadratic calibration algorithm to the desert and lunar data results in improved agreement in their long-term radiance trends. A clear understanding of the magnitude of the gain non-linearity could be useful to help improve the quality of numerous MODIS science products, including the land imaging applications that rely heavily on these bands.**

***Index Terms*—MODIS, reflective solar bands, nonlinear**

I. Introduction

THE Moderate Resolution Imaging Spectroradiometer (MODIS) flight model was launched on the Aqua satellite in May 2002 and has had very successful and stable operations on orbit [1], [2]. Aqua MODIS is a polar-orbiting whiskbroom imager, which acquires Earth images in 36 spectral channels from the visible through infrared. Together with its predecessor MODIS instrument aboard the Terra satellite, it produces a wide variety of environmental data products for the remote sensing and scientific user community. Twenty of the MODIS spectral bands are reflective solar bands (RSB) that measure the top-of-atmosphere (TOA) solar radiance reflected from the Earth over a wavelength range of 412 nm to 2250 nm and at three nadir spatial resolutions: 0.25 km, 0.5 km, and 1 km.

MODIS bands 1 (645 nm) and 2 (858 nm) image at the highest resolution of any MODIS bands, 250 m at nadir, which is achieved by using an along-track array of 40 detectors (compared to 10 detectors for the 1 km resolution bands) and acquiring four sub-samples of data along scan for each sample of the 1 km resolution bands. The center wavelength, bandwidth, and gain of bands 1 and 2 were designed to be suitable for a variety of land imaging applications, and they are critically important to several MODIS data products such as surface reflectance, BRDF/Albedo, and vegetation indices [3].

For each MODIS RSB detector, the detector gain was calibrated prior to launch, and the calibration is updated on orbit primarily using an on-board solar diffuser (SD). Since the MODIS gain can vary as a function of the angle of incidence (AOI) of light off the primary scan mirror (the response versus scan, or RVS function), the SD calibrations are combined with regular observations of the Moon and of pseudo-invariant calibration sites (PICS) in the Libyan desert [2], [4]. The calibration assumes a linear relationship between the observed top-of-atmosphere radiance and the background-subtracted instrument response for each detector. Any non-linear behavior in the detector or electronic responses can contribute to errors in the calibrated reflectance and radiance products, which can potentially have implications for all the science products that rely on these bands. Most RSB detectors continue to have very linear behavior even after more than 18 years of on orbit operation. However, there is evidence that the detectors in bands 1 and 2 have a non-linear component to their gain – different gain for different radiance levels – that has been changing in time during the mission.

The clearest evidence of non-linear gain comes from the on-board SD measurements. For Aqua MODIS, the SD calibrations are regularly performed at two different radiance levels by moving an attenuation screen in front of the SD. Linear gain calibration coefficients derived with the attenuation screen compared to those without the attenuation screen disagree with each other and that disagreement changes over the mission. There is also disagreement in how well the SD-based calibration works for different types of Earth scenes. For example, the calibration used in MODIS Collection 6 (C6) and previous Collections relied on the SD observations with screen open data combined with lunar observations to derive the on-orbit gains changes across all AOI. This calibration performed well near nadir, but performed less well near the beginning of the scan range when evaluated with desert and deep convective

K. A. Twedt, S. Henderson, A. Angal, and X. Geng are with Science Systems and Applications Inc, Lanham, MD 20706, USA (e-mails: kevin.twedt@ssaihq.com, sarah.henderson@ssaihq.com, amit.angal@ssaihq.com, xu.geng@ssaihq.com).

X. Xiong is with the Sciences and Exploration Directorate, NASA/GSFC, Greenbelt, MD 20771, USA (e-mail: xiaoxiong.xiong1@nasa.gov).

cloud (DCC) targets, mainly due to disagreement between the lunar and Earth scene radiance trends [5]. As a result, the Collection 6.1 (C6.1) calibration relies primarily on the desert data to determine long-term gain changes and does not use the lunar observations [6]. It has also been found that the SD calibrations performed with the screen closed (lower radiance) provide more stable calibration of ocean scenes, and the current calibration used by the NASA ocean biology processing group for the ocean color products uses the SD screen closed calibration as a baseline [7].

In this paper, we present evidence for non-linear gain changes of Aqua MODIS bands 1 and 2, which has not been well documented in the past, using data from both on-board calibrators and typical Earth scenes, and attempt to quantify the magnitude of the non-linearity. We review the linear calibration methodology that is currently used to generate the MODIS Collection 6 and 6.1 Level 1B (C6/C6.1 L1B) products for the RSB. Calibration results from the SD both with and without the attenuation screen are compared. Long-term radiance trends from lunar calibrations and typical desert and ocean scenes are also compared. We present a simple method for on-orbit characterization of the response non-linearity by combining the results of the two sets of SD calibrations and find deviations from linearity of up to 3% within the typical signal ranges. Applying a quadratic calibration algorithm to the desert and the lunar data results in an improved agreement in their long-term radiance trends. While the MODIS Level 1B calibration continues to be performed using a linear algorithm, a clear understanding of the magnitude of the non-linear impact could be used to help improve the quality of various MODIS science products that are derived from these bands.

II. RSB Calibration

A. Solar Diffuser Calibration

Here we review the methods used to calibrate the on-orbit gain and RVS that are currently used to derive the calibrated reflectance of the MODIS RSB in the NASA Collection 6.1 Level 1B (L1B) products, focusing on bands 1 and 2. The MODIS calibration is primarily based on observations of a sunlit solar diffuser. The TOA reflectance factor is determined from

$$\rho_{EV}\cos(\theta_{EV}) = \frac{m_1 dn^*_{EV}}{RVS_{EV}\, d^2_{ES}}, \quad (1)$$

where ρ_{EV} is the Earth view reflectance, θ_{EV} is the solar zenith angle, d_{ES} is the Earth-Sun distance, m_1 is a calibration coefficient, and RVS_{EV} is the response versus scan angle at the view angle of the Earth View (EV) pixel. The dn^*_{EV} term is the background-subtracted and temperature-corrected digital counts of the EV pixel, expressed as

$$dn^* = dn\left[1 + k_{inst}\left(T_{inst} - T_{ref}\right)\right], \quad (2)$$

where $dn = (DN - DN_{SV})$ is the background-subtracted digital counts, DN is the raw measured digital signal of each detector which is a 12-bit integer with values between 0 and 4095, DN_{SV} is the average DN when viewing the SV port which serves as a dark background reference, k_{inst} is a calibration coefficient determined from pre-launch measurements, T_{inst} is the instrument temperature for the current scan, and T_{ref} is a fixed reference temperature. Typically, the temperature correction, $k_{inst}(T_{inst} - T_{ref})$, is on the order of 1% or less for typical MODIS temperature ranges.

The SD calibrations are used to determine the calibration coefficient m_1 and track its on-orbit changes, following

$$m_1 = \frac{\rho_{SD}\cos(\theta_{SD})\Gamma_{SDS}\Delta_{SD} d^2_{ES}}{dn^*_{SD}}, \quad (3)$$

where Γ_{SDS} is the transmittance of the optional SD screen, θ_{SD} is the angle between the solar vector and SD surface normal, ρ_{SD} is the pre-launch measured bi-directional reflectance factor (BRF) of the solar diffuser, and Δ_{SD} is the on-orbit degradation of the SD BRF as measured by the on-board solar diffuser stability monitor (SDSM) [8], [9]. The Aqua SD calibrations are executed on a regular schedule, currently once every three weeks though the frequency has varied at different times in the mission. During normal MODIS operation, the SD door is kept closed to prevent unnecessary exposure of the SD to solar radiation and is only opened during the scheduled SD calibrations. An SD calibration can be performed with the SD screen either in the "open" position (without the SD screen in the optical path) or in the "closed" position (with the SD screen in the optical path).

For the C6 and C6.1 L1B calibration, the screen closed calibrations are used to derive the gain for the high gain ocean color bands 8-16 as these bands saturate with the screen open. The screen open calibrations are used for all other RSB, bands 1-7, 17-19 and 26, as the screen open calibration provides higher signal-to-noise in the measurements. The SD screen transmittance is about 7.6%. For most RSB that have unsaturated measurements with both screen closed and screen open, the on-orbit trends in m_1 calculated from the two sets of calibrations are in good agreement with each other. The only exceptions to this are bands 1 and 2, which have seen a divergence. Figure 1 shows the on-orbit change in the measured m_1 values calculated from the SD screen open compared to screen closed calibrations for bands 1-4. The two trends gradually diverge by about 2% over the mission for bands 1 and 2. This divergence is seen for every detector, subframe, and mirror side, though the exact magnitude and timing of the divergence varies from one detector to another. The divergence in the linear gain coefficient for calibrations performed at two different radiance levels indicates that the gain for these bands has a non-linear component that is changing in time. By contrast, the screen open and screen closed calibrations for bands 3 and 4 are in very good agreement with each other over the entire mission. Bands 1 and 2 are also atypical in that they

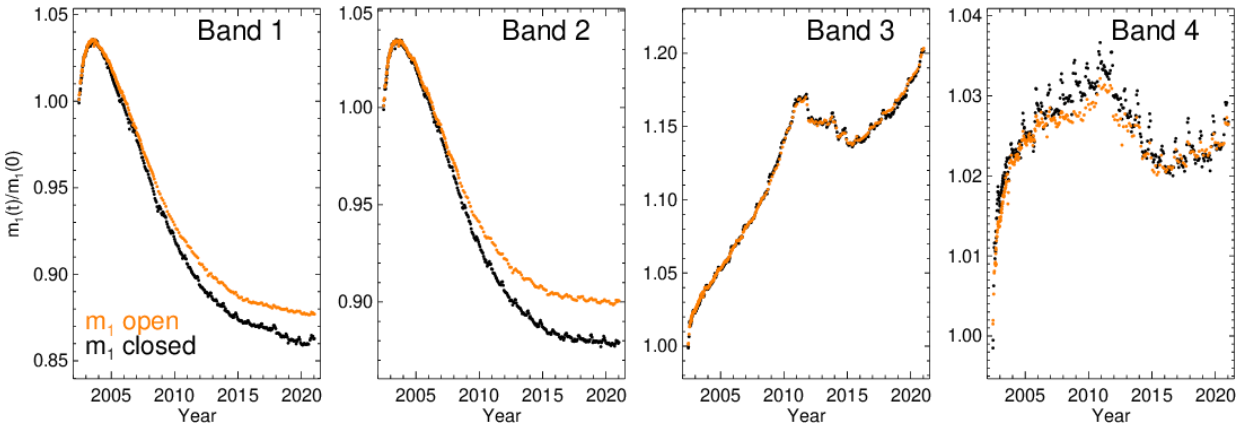


Fig. 1. Calibration coefficient m_1 over the mission, normalized to the value at the mission start, from SD calibrations with the screen open compared to those with the screen closed for bands 1, 2, 3 and 4. Results are averaged over all detectors, subframes, and mirror sides within a band.

have seen a 10% to 15% decrease in m_1 over the mission, which implies an increase in the overall gain of the instrument. The source of this gain increase remains a mystery, as it cannot be explained by optical changes and has also not been observed in the regularly performed electronic calibrations [10].

B. RVS calibration

The solar diffuser allows measurement of the gain change at only one AOI of light off the MODIS primary scan mirror. To track how the gain changes as a function of AOI, additional calibration sources need to be included. The RVS for MODIS RSB is calibrated using a combination of SD, lunar, and desert data, depending on the band. Lunar observations have been made on a near-monthly basis over the entire mission and provide a very stable measure of on-orbit gain changes [11]. The lunar observations are made through the space view port at a different AOI than the SD measurements. For most RSB, the SD observations determine the gain at the SD AOI, the lunar observations determine the *relative* on-orbit gain change at the SV AOI (only SD calibrations can provide accurate *absolute* gain calibration), and a linear extrapolation is used to derive the gain across all AOI. For some bands, this linear function is not sufficient to accurately track the RVS changes. Starting in Collection 6, data from pseudo-invariant calibration sites (PICS) in the Libya desert were used to help calibrate the RVS of bands 8 and 9, the shortest-wavelength bands [4]. Initially in C6, all other RSB, including bands 1 and 2, continued to use the SD-lunar linear RVS calibration.

After continued monitoring of the desert reflectance trends for bands 1-4, it was found that the C6 reflectance measured both from the Libya desert, as well as from deep convective clouds (DCC), had drifts for bands 1 and 2, particularly near the beginning of scan where the lunar trends set the calibration [5]. To address this problem, the calibration algorithm using the desert PICS to derive the gain trends was extended to bands 1-4 in Collection 6.1 [6]. This followed the precedent set by Terra MODIS, which used the desert-based calibration for bands 1-4, 8, and 9 in the initial C6 calibration (and continued in C6.1).

In the desert-based calibration, the on-orbit change in the signal from Libya desert sites is tracked at multiple viewing angles in order to capture the shape of the gain change with AOI (the RVS). For the shortest-wavelength bands (bands 8 and 9) there is a slight discrepancy between the SD trend and the desert trends near the SD AOI, which is thought to be due to the inability of the SDSM to accurately track the SD degradation as it is viewed by the MODIS detectors. As a result, the on-orbit trend from the desert is used to replace the on-orbit SD trend to provide the most accurate calibration. The lunar calibration, however, is still considered to be the most reliable calibration source as it has better long-term stability than the SD or an Earth target, and it has less variation than the desert scenes. For bands 8, 9, 3, and 4, the lunar trends and desert trends at similar AOI are in fairly good agreement with each other; therefore, the desert-based calibration for these bands is still constrained to match the lunar-based gain at the lunar AOI. For bands 1 and 2, the disagreement between the desert and lunar trends is an unresolved problem. As a result, the C6.1 calibration relies only on the SD and desert and does not use the lunar data. In the next Section, we explore the role of signal level in determining the reflectance/radiance trends observed from different calibration sources.

III. Reflectance Comparisons

The detector signal level for any band varies greatly over the Earth as the radiance of the scene changes. Figure 2 shows an overview of the typical ranges of measured signal levels for bands 1 and 2 for various calibration targets, including the SD, Moon, and desert and ocean scenes. For all of these targets, the observed dn values change over the mission as the gain of the MODIS bands changes. The ranges shown in Figure 2 are based roughly on the typical signal levels observed in year 2020, though the on-orbit gain change for bands 1 and 2 is only up to 12%, so the typical dn is only slightly shifted at different times in the mission, and the relative dn difference between the scenes is the same. For the desert and ocean scenes, there can be a significant variation in signal levels depending on the time of year, solar illumination angles, and satellite viewing angles. By design, the SD signal level with the screen closed is generally similar to typical ocean scenes, and the SD signal level with the screen open is generally similar to bright land scenes and clouds.

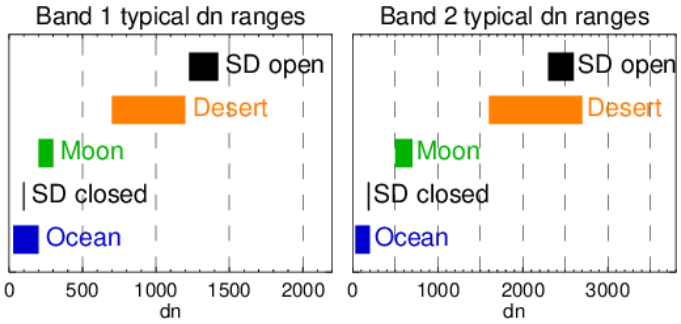


Fig. 2. Typical ranges of measured signal levels, dn, for different scenes for band 1 (left) and band 2 (right).

If the relationship between scene TOA radiance and measured dn is linear, then a calibration derived using the relatively high radiance SD with screen open should be able to be applied accurately to any scene. If this relationship has any non-linear features, then the calibration should still be reasonably accurate when the calibration source and the observed scene are at similar radiance levels, but the accuracy is likely to be worse for scenes with radiance far from the calibration source radiance. To demonstrate this, we examine the on-orbit reflectance trends from typical desert and ocean scenes using both the SD screen open and SD screen closed calibrations.

For the desert scenes, we use reflectance trends from the Libya 4 site, a very stable common reference site for calibration of remote sensing instruments. The Aqua satellite makes repeated passes over this site at the same view angle once every 16 days. We focus on observations centered on frame 997 of the EV image, corresponding to an AOI of 51° since this is very close to the 50.25° AOI at which the SD observations are made. For this view angle, the SD calibration can be applied directly to the Earth scene data without worrying about the accuracy of the RVS. The reflectance for each desert observation is averaged over a 20 by 20 km^2 region and a semi-empirical BRDF correction is applied. This is the same data and processing scheme that is used for the desert-based corrections to the instrument gain and RVS in the C6/6.1 calibration algorithm [4].

Figure 3 shows the reflectance trends of Libya 4 normalized to mission start for bands 1 and 2, averaged over all detectors, using both the screen open and screen closed calibrations. Linear fit lines show the magnitude of the mission drift in reflectance for each of the calibration versions. For both bands 1 and 2, the screen open calibration results in a very stable reflectance trend, but the screen closed calibration results in a downward drift in reflectance of about 2% for band 1 and about 3% for band 2.

For the ocean scenes, we use an interband calibration methodology previously presented [12]. It is based on the fact that there is a high correlation in the reflectance between the spectral matching MODIS bands: band 1 (645 nm) and band 13 (667 nm), and band 2 (858 nm) and band 16 (870 nm). Assuming the calibration for bands 13 and 16 are accurate, we can evaluate the reflectance trends of bands 1 and 2 using bands 13 and 16 as the reference.

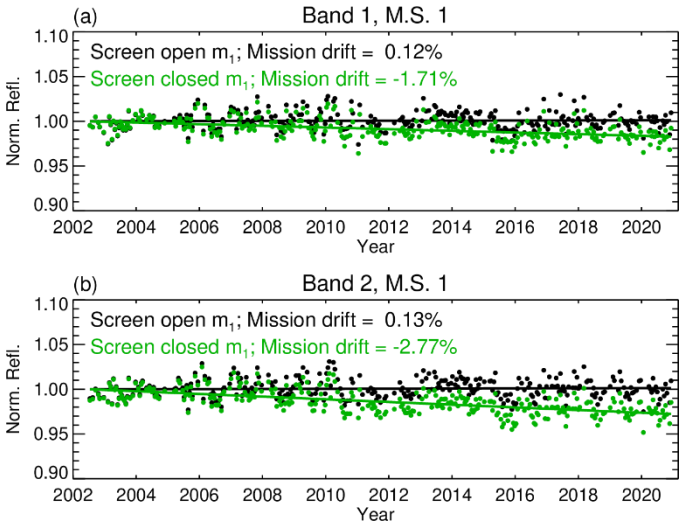


Fig. 3. Normalized reflectance of Libya 4 desert site at an AOI of 51° (near the SD AOI) for (a) band 1 and (b) band 2 mirror side 1 using the SD calibration with the screen open compared to the screen closed.

The ocean scene data used in this work are collected from the North Atlantic Ocean centered around the coordinates 24° N, -42° E with a frequency of once every 16 days through the Aqua mission. The data centered at frame 978 (the SD AOI) and within 15 frames are collected across the scans in each granule. The data from bands 1 and 2 are aggregated to 1 km spatial resolution to match the pixel size of bands 13 and 16. The matching pair is excluded if any of the two pixels in the pair is saturated. The data from the first year are used to derive a linear relation between the spectral matching bands, which can be described as

$$\rho_t = k * \rho_r + b, \tag{4}$$

where ρ_t is the TOA reflectance of bands 1 and 2, ρ_r is the TOA reflectance of the reference bands 13 and 16, k is the slope, and b is the offset. Using the derived linear coefficients, the true reflectance for each aggregated bands 1 and 2 pixel can be estimated from the reflectance of the matching pixel in bands 13 and 16, respectively. The normalized reflectance, $\rho_t/(k * \rho_r + b)$, is then averaged over all valid pixels for each detector and mirror side of bands 1 and 2 for each granule. Figure 4 shows the normalized reflectance averaged over all detectors for bands 1 and 2 over the mission, again using both the screen open and screen closed calibrations. The data gaps in the plots are due to the sun glint impact, which results in too few valid pixels in the high gain reference bands. In contrast to the desert trends in Figure 3, the ocean trends in Figure 4 show that the screen closed calibration results in flat reflectance trends on-orbit for both bands. The screen open calibrations in this case perform poorly, resulting in upward reflectance drifts of about 2% and 3% for bands 1 and 2 respectively.

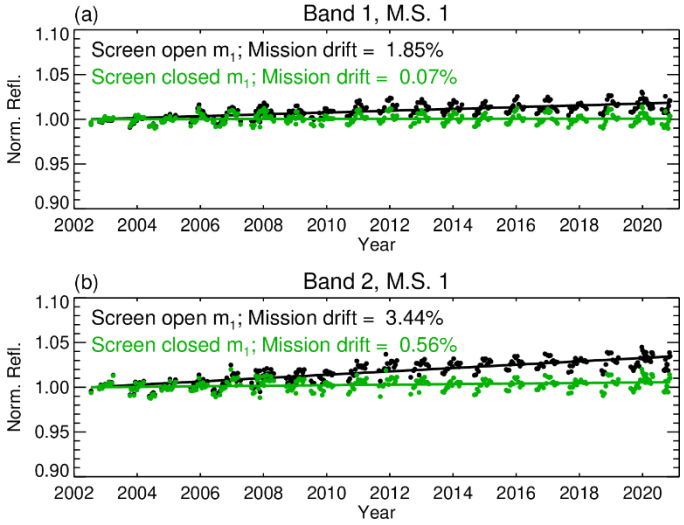


Fig. 4. Normalized reflectance of ocean scene at the SD AOI calculated using the interband calibration for Aqua bands 1 (a) and 2 (b) mirror side 1 using the SD calibration with the screen open compared to the screen closed.

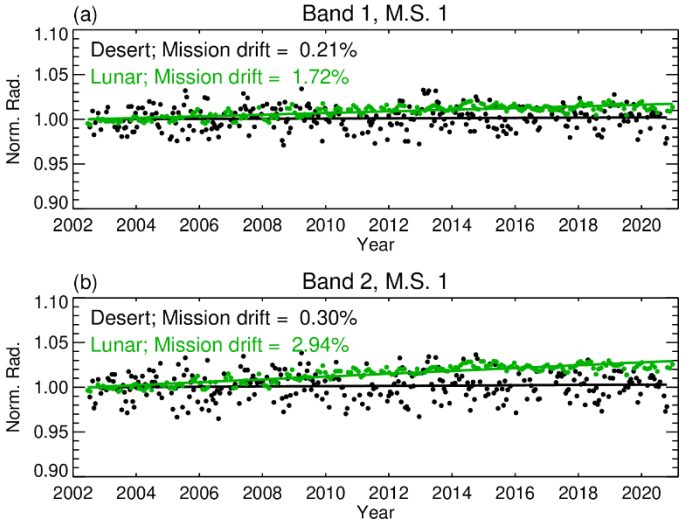


Fig. 5. Normalized radiance of the Libya 4 site compared to normalized radiance of lunar observations at a similar AOI for Aqua bands 1 and 2. The radiance is calculated using mission-reprocessed m_1 and RVS LUTs using C6.1 algorithm as described in Section 2.

The superior performance of the screen open calibration on the desert reflectance and the screen closed calibration on the ocean reflectance is a clear indication that both sets of SD calibrations are accurate, so long as they are applied to Earth scenes with similar typical signal levels. This is likely also the case for the discrepancy we see in the lunar and desert data used for calibration, as mentioned in Section 2. Since the lunar data is collected at a frame near the beginning of scan, we cannot directly calculate the lunar radiance trends from the SD calibrations alone, and the effect of the RVS needs to be included. The RVS used in C6.1 is derived entirely from the desert data, so we assume that this is accurate since it is derived entirely from scenes with a similar radiance level. To illustrate the lunar-desert disagreement, we calculate the lunar radiance and the desert radiance at a comparable frame to the lunar frame using screen open m_1 and mission reprocessed RVS LUTs based on the desert data. These m_1 and RVS LUTs are consistent with, though not exactly the same as, the C6.1 L1B calibration. The lunar observations are processed taking into account changes in viewing geometry and lunar phase as described previously [11], and the desert radiance trend is again from the Libya 4 site, this time for observations centered on frame 43. Figure 5 shows the comparison of lunar and desert long-term radiance trends. While the desert trends are very stable, the lunar radiance shows clear upward drifts of 2-3%.

Similarly, we can reproduce the plots in Fig. 5 using the screen closed m_1 trends and the same desert-derived RVS, and the result would show a relatively flat trend for the lunar radiance and a downward drift in reflectance for the desert trends. This is consistent with the idea that the screen closed calibration works well for the targets with lower typical dn levels, like the lunar data, and the screen open calibration works well for targets with higher typical dn levels, like the desert. But the desert and lunar observations cannot be combined to reliably derive a single RVS function.

IV. Quadratic Calibration Algorithm

Throughout the Aqua MODIS mission, SD screen open and screen closed calibrations have been routinely run in pairs: one orbit with the SD screen closed and a consecutive orbit with the SD screen open. The measurements only probe the gain at two different radiance levels, so they give limited ability to probe any non-linear gain behavior, which could be a complicated function of radiance. However, we can combine the measurements from the two near-coincident calibrations to give an estimate of how the radiance and signal level are related and how that relationship changes with time. In this Section, we use the SD calibration pairs to derive both linear and quadratic gain coefficients for bands 1 and 2. In place of (1), we define the reflectance calibration equation as

$$\rho_{EV}\cos(\theta_{EV}) = \frac{(c_1 dn_{EV} + c_2 dn_{EV}^2)[1+k_{inst}(T_{inst}-T_{ref})]}{d_{ES}^2} = \frac{c_1 dn_{EV}^{*}\left(1+\frac{c_2}{c_1}dn_{EV}\right)}{d_{ES}^2}, \quad (5)$$

where c_1 and c_2 are calibration coefficients. For the quadratic calibration algorithm, we denote the linear coefficient as c_1 to distinguish it from the m_1 used in the linear-only calibration algorithm. Obviously, there are many other choices of two-coefficient functions that we could use to relate reflectance to dn. For example, the simplest variant would be to have a polynomial with constant and linear terms instead of linear and quadratic terms. We have chosen to use the functional form of (5) based partly on the experience of the Visible Infrared Imaging Radiometer Suite (VIIRS), which also uses a polynomial function with no constant term to relate the reflectance to dn [13], [14]. Since the temperature dependence was determined pre-launch for a linear calibration, we have no knowledge of how a quadratic calibration term might depend on temperature, so in (5) we choose to apply the same

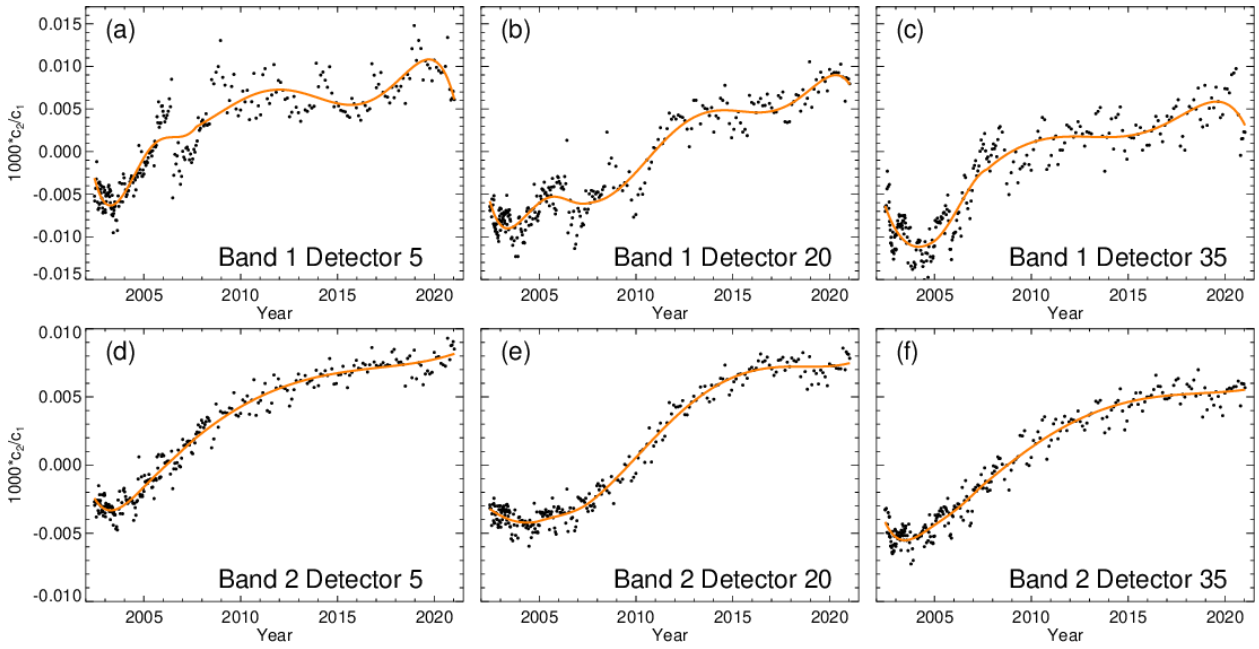


Fig. 6. Results of $1000 * c_2/c_1$ as a function of time for different detectors of bands 1 and 2. Black points are measured values from each open/closed calibration pair, averaged over all four subframes and both mirror sides, and orange solid lines are empirical fits to the data.

temperature correction equally to both terms.

To derive c_1 and c_2 from the SD calibrations, we make the assumption that the transmittance of the screen is constant in time throughout the entire Aqua mission. While the screen transmittance Γ_{SDS} does have slight variations with incident solar angle, the difference in the value of Γ_{SDS} between data collected in two consecutive orbits is negligible. We also assume that the changes in Earth-Sun distance and in SD BRF are negligible between two consecutive orbits. Thus, the only difference between the SD radiance in the screen open compared to the screen closed orbits is the screen transmittance, and we can use (5) to write

$$\frac{L_{SD,open}}{L_{SD,close}} = \frac{1}{\Gamma_{SDS}} = \frac{dn^*_{open}\left(1+\frac{c_2}{c_1}dn_{open}\right)}{dn^*_{closed}\left(1+\frac{c_2}{c_1}dn_{closed}\right)}. \quad (6)$$

Rearranging (6), we solve for the ratio of c_2/c_1:

$$\frac{c_2}{c_1} = \frac{\Gamma_{SDS}dn^*_{open} - dn^*_{closed}}{dn^*_{closed}dn_{closed} - \Gamma_{SDS}dn^*_{open}dn_{open}}. \quad (7)$$

The values of the screen transmittance for a given calibration pair is based on a function of the solar angles determined from early-mission yaw maneuver data [15]. The temperature correction is applied to the open and closed data based on the instrument temperature during each orbit individually. We calculate the values of c_2/c_1 for each detector, mirror side, and subframe of Aqua MODIS bands 1 and 2 for each pair of open/closed calibrations over the mission. Figure 6 shows the results for a few example detectors, with detector number based on the L1B product detector order. The results are plotted as $1000 * c_2/c_1$ to place the values on a more intuitive scale: this represents the fractional magnitude of the nonlinear term for a scene signal level of $dn = 1000$.

For both bands 1 and 2, there is a clear increase in the size of the nonlinear term over the mission, with a change in magnitude on the order of 1-2% for a $dn = 1000$ level signal. In order to provide smooth time trends, we fit the c_2/c_1 measurements for each detector to an empirical function of time: a piece-wise polynomial function with smoothly connected segments. The fits are shown as the solid orange lines in Fig. 6. Most detectors show a non-zero value of c_2/c_1 at the beginning of the mission. This could be an indication that there was significant gain non-linearity even at time of launch, or it could simply mean that the screen transmittance function determined from yaw maneuver data is not precise. In either case, our focus is on the on-orbit change in the calibration coefficients, rather than the absolute magnitude.

Though there is a clear overall increase in c_2/c_1 over time for every detector, there is some variation in the timing of the trends between detectors. Figure 7 shows the on-orbit change in c_2/c_1 as a function of detector position (L1B product order) at four different times in the mission. For both bands 1 and 2, there is a common systematic spatial dependence to the nonlinear change. Early in the mission, the detectors near both edges have the most change and detectors near the center have almost no change. Mid-mission, the detectors near the center of the array have a much larger rate of change and end up with a larger overall on-orbit change than the edge detectors by year 2015. In the years between 2015 and 2021, there has been minimal change in the behavior for any detectors.

With the fitted values of c_2/c_1 derived using the data of both open and closed calibrations, the c_1 coefficient can be calculated using either open or closed SD calibration data using

$$c_1 = \frac{\rho_{SD}\Gamma_{SDS}\Delta_{SD}d_{ES}^2}{dn^*_{SD}\left(1+\frac{c_2}{c_1}dn_{SD}\right)}. \quad (8)$$

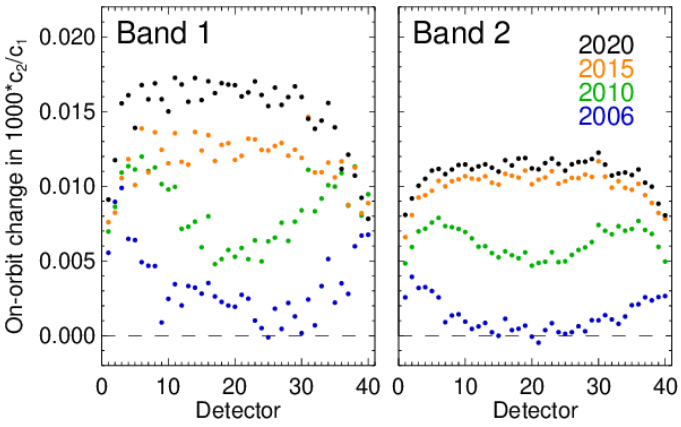


Fig. 7. On-orbit change in $1000 * c_2/c_1$ as a function of detector position for bands 1 and 2 at four different years in the mission: 2006, 2010, 2015, and 2020. The on-orbit change is calculated by taking the average measured c_2/c_1 for each year minus the average measured c_2/c_1 for year 2002 (first year of mission). Points are the average over all four subframes and both mirror sides for each detector.

We use the screen open calibrations to calculate c_1 since these give better signal-to-noise in the measurements. Examples of the c_1 trends are show in Fig. 8 for bands 1 and 2 compared to both the screen open and screen closed m_1 trends generated with the linear calibration algorithm (Fig. 1). The values of c_1 are similar in magnitude to the screen closed m_1 trends as expected, since they both represent the calibration for small signal levels. The c_1 trends are smoother than the screen closed m_1 trends since they are calculated with the screen open data and the fitted c_2/c_1 trends.

With this quadratic reflectance equation and the SD-derived c_1 and c_2/c_1 coefficients, we can use a single calibration approach to recalculate the reflectance and radiance of the other standard calibration targets. The normalized desert reflectance and normalized lunar radiance are recalculated using the quadratic gain coefficients. For the lunar radiance, the lunar images are reprocessed using the nonlinear calibration applied to the dn at the individual pixel level. For the desert reflectance, the dn values are averaged over the site and the non-linear equation is applied to the averaged dn. The same BRDF correction is applied as before. The RVS used is the same RVS that was used in Section 3 to generate Fig. 5, derived using data only from the desert sites. The comparison of desert and lunar normalized radiance trends with quadratic calibration is shown in Fig. 9. Contrasting to Fig. 5, the trends are now both stable over the mission and in agreement with each other. The ocean scene reflectance trends could also be recalculated using the quadratic calibration algorithm (not shown). Since the ocean scenes have such low dn, the c_2 term is almost negligible and therefore we expect the long-term reflectance trends to be within 0.3% of the values shown in Fig. 4 that use SD screen closed calibration only.

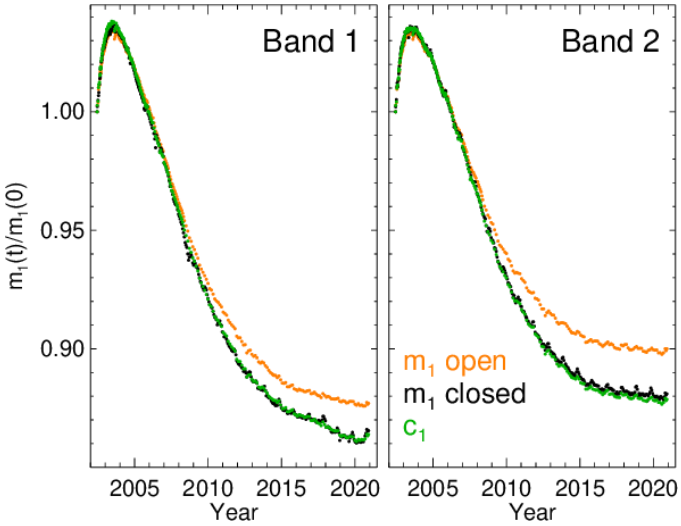


Fig. 8. Results of c_1 as a function of time for band 1 and band 2 compared to the m_1 from the linear calibration from both screen open and screen closed SD calibrations. Results are averaged over all detectors, subframes, and mirror sides within a band.

MODIS has used a linear gain calibration in the NASA L1B products for all RSB since the beginning of the mission and the plan is to continue to use linear gain calibration in the next MODIS Collection, Collection 7, which is currently under development. However, knowledge of quadratic gain coefficients derived from the SD could still prove useful for testing the impact of the bands 1 and 2 non-linear performance on downstream science products. It is straightforward to relate the L1B reflectance product calculated with the linear calibration in (1), ρ_{L1B}, to the reflectance product that would be obtained using the quadratic algorithm of (5), ρ_{quad}. By solving (1) for dn^*_{EV} and substituting into (5), we can relate ρ_{quad} to ρ_{L1B} as

$$\rho_{quad} = \rho_{L1B}\left[\frac{c_1}{m_1}\right]\left(1 + \frac{c_2}{c_1}\left[\frac{\rho_{L1B}\cos(\theta_{EV}) * RVS}{m_1 d_{ES}^2}\right]\right). \quad (9)$$

In the quadratic reflectance equation, the $dn_{EV}c_2/c_1$ term is much smaller than one for the entire range of possible dn values, so any small variation in dn will have a negligible impact on the $1 + dn_{EV}c_2/c_1$ term. We have used this

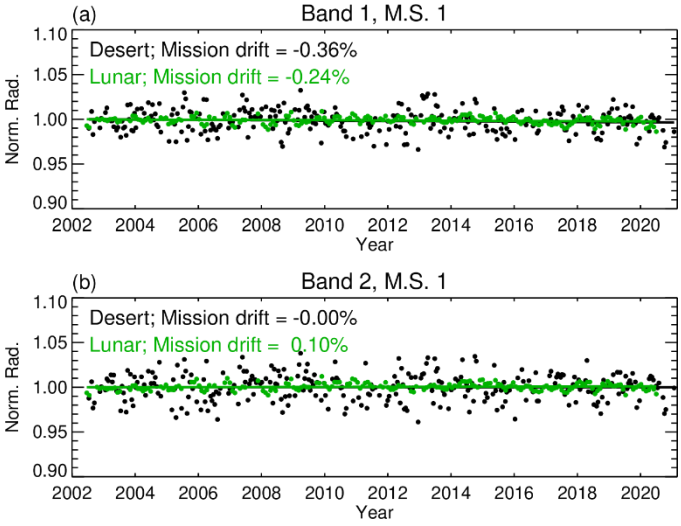


Fig. 9. Normalized radiance of the Libya 4 site compared to normalized radiance of lunar observations at a similar AOI for Aqua bands 1 and 2. Similar to Fig. 5, except the radiance for both datasets is calculated using mission-reprocessed c_1 and c_2 LUTs from the quadratic calibration equation.

assumption in deriving Eq. 8 to ignore the impact of the temperature correction on the quadratic term, i.e. $1 + dn_{EV}^{*} c_2/c_1 \approx 1 + dn_{EV} c_2/c_1$. Likewise, we can further simplify (9) by noting that d_{ES}^2 varies from unity by only about 6% at any point in time, and RVS varies from unity by only a few percent over the mission lifetime for bands 1 and 2 at any AOI, giving

$$\rho_{quad} = \rho_{L1B} \frac{c_1}{m_1} \left(1 + \frac{c_2}{c_1 m_1} \rho_{L1B} \cos(\theta_{EV})\right). \quad (10)$$

Equation 10 could be very useful, as it allows one to convert the L1B reflectance factor to a new reflectance factor based on the quadratic gain algorithm using only the calibration coefficient LUTs and without having to go back to the original raw signal data in the Level 1A product. In this way, the impact of quadratic calibration on downstream science products could potentially be tested without having to alter the L1B algorithm or data. It is unclear exactly how successful this quadratic calibration would be at correcting the impact of the non-linear gain performance on reflectance/radiance products for general scenes. The derived values of the c_1 and c_2/c_1 gain coefficients have fairly low uncertainty due to the good signal-to-noise of the SD calibrations, as evidenced by the low short-term variance in the data points in Fig. 6 and Fig. 8. For scenes with typical radiance near one of the two SD tie points, we estimate the on-orbit gain trends from the quadratic calibration to be accurate to within 0.5%, and they should provide an improvement over the current linear calibration used in the L1B. However, the true relationship between observed radiance and dn could have a complicated functional form that is not well modeled by a simple quadratic function, and the shape of that function could evolve over time. For scenes with typical radiance far from the two SD tie points, the on-orbit gain trends from the quadratic calibration could potentially still have inaccuracies up to a few percent.

V. Discussion and Summary

The source of the observed gain non-linearity in Aqua MODIS bands 1 and 2 is not known but is presumably due to some non-ideal performance of either the individual detectors or subsequent electronics. The clear spatial dependence – the systematic variation of the quadratic gain coefficients with detector position – seen in Fig. 7 suggests that the detectors themselves, or some properties of the focal plane array, are responsible for the non-linear behavior. Problems with the downstream electronics, for example the analog-to-digital converters, would be expected to affect each detector in the same way, since all detectors in each band are read out in serial through the same channels. The spatial dependence of the quadratic gain term is very similar to the spatial dependence observed in the linear gain term (m_1) in the regular screen open calibrations, suggesting that a common component is possibly causing both the unusual 10% to 15% gain increase seen by these two bands over the mission as well as the deviations from linearity. Previous work found slight on-orbit degradation of the modulation transfer function for Aqua MODIS bands 1 and 2, which may also be connected [16], [17].

There are also some indications of different types of nonlinear behavior in different radiance ranges. The NASA ocean color products have a linearity correction applied to them based on previous work aimed at reducing image striping [18]. That work found radiance-dependent gain differences between the four subframes of bands 1 and 2 over dark ocean scenes, covering a radiance range extending lower than the SD screen closed observations. In our work, we do not find any significant differences between the four subframes in the c_1 or c_2/c_1 coefficients derived from the SD open and closed data, which suggests that there may be a different mechanism causing deviations from gain linearity at very low radiance.

For Terra MODIS bands 1 and 2, a similar discrepancy is seen between the lunar and desert radiance trends using the C6.1 calibration, and there could very likely be non-linear gain changes on orbit similar to those observed for Aqua. However, the SD screen on Terra MODIS has been fixed in the closed position since July 2003, early in the Terra MODIS mission. The analysis we have used for Aqua MODIS relying on the SD screen open versus screen closed data is not possible for Terra, and alternative methods of non-linear gain characterization would have to be employed. The similar behavior between Terra and Aqua MODIS also suggests that the non-linear behavior relates to something inherent in the MODIS design rather than any specific pre-launch or on-orbit event.

One possibility to further study non-linear gain changes on either Aqua or Terra MODIS is through the use of measurements from the on-orbit spectroradiometric calibration assembly (SRCA), a unique on-orbit instrument capable of preforming radiometric, spectral, and spatial calibrations of MODIS on-orbit [19], [20]. The SRCA uses a set of halogen lamps and a movable neutral density filter to perform radiometric calibrations at multiple radiance levels, and these calibrations have been performed at regular intervals throughout the MODIS mission. However, changes in the radiance of the lamps on-orbit make it challenging to use the SRCA data to track changes in gain accurately, so this analysis is reserved for future work. The SRCA, though, has successfully monitored the relative spectral response (RSR) of all Aqua MODIS RSB regularly over the mission, showing very stable performance. It is therefore unlikely that the scene-dependent reflectance trends of bands 1 and 2 can be attributed to on-orbit RSR changes [21].

Observations of solar eclipse events on the calibration diffusers have recently been shown to be useful in verifying non-linear gain behavior for the Landsat 8 Operational Land Imager [22] and the Visible Infrared Imaging Radiometer Suite [23]. Since the SD door on Aqua MODIS is kept closed except during scheduled SD calibrations, the Aqua MODIS SD has not observed any solar eclipse events over its lifetime, though there may be the potential to observe future events.

In addition to the calibration scenes we evaluated in Section 3, deep convective clouds offer another pseudo-invariant Earth scene with high radiance that can assist in validation of gain linearity. For Aqua MODIS, band 2 exhibits partial saturation when viewing DCC, but the reflectance trends for band 1 have been carefully studied and generally agree well with the desert trends [24]. Scene-dependent gain effects have also been studied using ray-matched Earth observations from multiple

sensors covering wide radiance ranges [25], and these techniques could be further explored.

In summary, we present evidence of deviations from gain linearity in Aqua MODIS bands 1 and 2 of up to 3% by carefully comparing the reflectance and radiance trends of calibration targets and stable Earth scenes over a range of typical radiance levels. By combining the solar diffuser calibrations performed with and without the attenuation screen, we derive coefficients for a quadratic calibration algorithm and show that this calibration can be used to remove a previously observed discrepancy between lunar and desert radiance trends that are typically used for calibration. The quadratic calibration coefficients may be useful in estimating the impact of the non-linear gain on downstream MODIS land products.

ACKNOWLEDGMENT

We thank other past and present members of the NASA MODIS Characterization Support Team for their work on Aqua pre-launch and on-orbit calibration, and we thank Aisheng Wu for a technical review of this manuscript.

REFERENCES

[1] W. L. Barnes and V. V. Salomonson, "MODIS: a global imaging spectroradiometer for the Earth Observing System," in *Proceedings of SPIE*, Nov. 1992, vol. 10269, p. 102690G, doi: 10.1117/12.161578.

[2] X. Xiong *et al.*, "MODIS Reflective Solar Bands On-Orbit Calibration and Performance," *IEEE Trans. Geosci. Remote Sens.*, vol. 57, no. 9, pp. 6355–6371, 2019, doi: 10.1109/TGRS.2019.2905792.

[3] C. O. Justice *et al*., "The Moderate Resolution Imaging Spectroradiometer (MODIS): land remote sensing for global change research," *IEEE Trans. Geosci. Remote Sens.*, vol. 36, no. 4, pp. 1228–1249, Jul. 1998, doi: 10.1109/36.701075.

[4] J. Sun, X. Xiong, A. Angal, H. Chen, A. Wu, and X. Geng, "Time-Dependent Response Versus Scan Angle for MODIS Reflective Solar Bands," *IEEE Trans. Geosci. Remote Sens.*, vol. 52, no. 6, pp. 3159–3174, Jun. 2014, doi: 10.1109/TGRS.2013.2271448.

[5] R. Bhatt *et al.*, "Characterizing response versus scan-angle for MODIS reflective solar bands using deep convective clouds," *J. Appl. Remote Sens.*, vol. 11, no. 1, p. 016014, Jan. 2017, doi: 10.1117/1.JRS.11.016014.

[6] A. Angal, X. Xiong, A. Wu, X. Geng, and H. Chen, "Improvements in the On-Orbit Response Versus Scan Angle Characterization of the Aqua MODIS Reflective Solar Bands," *IEEE Trans. Geosci. Remote Sens.*, vol. 56, no. 3, pp. 1728–1738, Mar. 2018, doi: 10.1109/TGRS.2017.2767206.

[7] S. Lee, G. Meister, and B. Franz, "MODIS Aqua Reflective Solar Band Calibration for NASA's R2018 Ocean Color Products," *Remote Sens.*, vol. 11, no. 19, p. 2187, Sep. 2019, doi: 10.3390/rs11192187.

[8] X. Xiong, A. Angal, J. Sun, T. Choi, and E. Johnson, "On-orbit performance of MODIS solar diffuser stability monitor," *J. Appl. Remote Sens.*, vol. 8, no. 1, pp. 083514–083514, 2014.

[9] E. J. Aldoretta, K. A. Twedt, A. Angal, H. Chen, and X. Xiong, "On-orbit performance of the Terra and Aqua MODIS solar diffuser stability monitor," in *Proceedings of SPIE*, Sep. 2018, vol. 10764, p. 107641O, doi: 10.1117/12.2321163.

[10] X. Xiong, N. Chen, Y. Li, and T. Wilson, "Assessments and applications of Terra and Aqua MODIS on-orbit electronic calibration," in *Proceedings of SPIE*, Sep. 2016, vol. 9972, p. 99720X, doi: 10.1117/12.2238603.

[11] J.-Q. Sun, X. Xiong, W. L. Barnes, and B. Guenther, "MODIS Reflective Solar Bands On-Orbit Lunar Calibration," *IEEE Trans. Geosci. Remote Sens.*, vol. 45, no. 7, pp. 2383–2393, Jul. 2007, doi: 10.1109/TGRS.2007.896541.

[12] X. Geng, A. Angal, Y. Li, K. A. Twedt, and X. Xiong, "Improvements in the on-orbit response versus scan-angle characterization for the MODIS ocean color bands," in *Proceedings of SPIE*, Oct. 2019, vol. 11151, p. 1115124, doi: 10.1117/12.2532081.

[13] X. Xiong *et al.*, "VIIRS on-orbit calibration methodology and performance," *J. Geophys. Res. Atmospheres*, vol. 119, no. 9, pp. 5065–5078, May 2014, doi: 10.1002/2013JD020423.

[14] T. Choi, X. Shao, and C. Cao, "On-orbit radiometric calibration of Suomi NPP VIIRS reflective solar bands using the Moon and solar diffuser," *Appl. Opt.*, vol. 57, no. 32, p. 9533, Nov. 2018, doi: 10.1364/AO.57.009533.

[15] X. Xie, X. Xiong, D. Moyer, J. Sun, X. Liu, and W. Barnes, "Analysis of MODIS solar diffuser screen vignetting function," in *Proceedings of SPIE*, Aug. 2005, p. 58820T, doi: 10.1117/12.615394.

[16] T. Choi, N. Che, and X. Xiong, "On-orbit aqua MODIS modulation transfer function trending in along-scan from the Spectro-Radiometric Calibration Assembly," in *Proceedings of SPIE*, Aug. 2008, vol. 7081, p. 70810A, doi: 10.1117/12.793844.

[17] Zhipeng Wang, Xiaoxiong Xiong, Taeyoung Choi, and D. Link, "On-Orbit Characterization of MODIS Modulation Transfer Function Using the Moon," *IEEE Trans. Geosci. Remote Sens.*, vol. 52, no. 7, pp. 4112–4121, Jul. 2014, doi: 10.1109/TGRS.2013.2279610.

[18] G. Meister, C. Pan, F. S. Patt, B. Franz, X. Xiong, and C. R. McClain, "Correction of subframe striping in high resolution MODIS ocean color products," in *Proceedings of SPIE*, Sep. 2007, vol. 6677, p. 66770P, doi: 10.1117/12.732191.

[19] T. Choi, X. Xiong, Z. Wang, and D. Link, "Terra and Aqua MODIS on-orbit spectral characterization for reflective solar bands," in *Proceedings of SPIE*, Jun. 2013, vol. 8724, p. 87240Y, doi: 10.1117/12.2016640.

[20] D. Link, Z. Wang, K. A. Twedt, and X. J. Xiong, "Status of the MODIS spatial and spectral characterization and performance after recent SRCA operational changes," in *Proceedings of SPIE*, Sep. 2017, vol. 10402, p. 104022G, doi: 10.1117/12.2273053.

[21] K. A. Twedt, A. Angal, and X. Xiong, "Effects of out-of-band and time-varying relative spectral response on the calibration of MODIS reflective solar bands," *J. Appl. Remote Sens.*, vol. 14, no. 02, p. 024523, Jun. 2020, doi: 10.1117/1.JRS.14.024523.

[22] R. Morfitt *et al.*, "Landsat-8 Operational Land Imager (OLI) Radiometric Performance On-Orbit," *Remote Sens.*, vol. 7, no. 2, pp. 2208–2237, Feb. 2015, doi: 10.3390/rs70202208.

[23] K. A. Twedt, N. Lei, and X. Xiong, "Using solar eclipse events to validate VIIRS reflective solar band calibration at multiple radiance levels," in *Proceedings of SPIE*, Oct. 2019, vol. 11151, p. 111511M, doi: 10.1117/12.2532855.

[24] A. Angal, X. Xiong, Q. Mu, D. R. Doelling, R. Bhatt, and A. Wu, "Results From the Deep Convective Clouds-Based Response Versus Scan-Angle Characterization for the MODIS Reflective Solar Bands," *IEEE Trans. Geosci. Remote Sens.*, vol. 56, no. 2, pp. 1115–1128, Feb. 2018, doi: 10.1109/TGRS.2017.2759660.

[25] D. R. Doelling *et al*., "MTSAT-1R Visible Imager Point Spread Correction Function, Part I: The Need for, Validation of, and Calibration With," *IEEE Trans. Geosci. Remote Sens.*, vol. 53, no. 3, pp. 1513–1526, Mar. 2015, doi: 10.1109/TGRS.2014.2344678.